Cullin3-RING ubiquitin ligases are intimately linked to the unfolded protein response of the endoplasmic reticulum

Kyungho Kim[1], Sujin Park[2], and Jinoh Kim[2,] *

[1] Specific Organs Cancer Branch, National Cancer Center, Goyang, Gyeonggi 10408, Republic of Korea

[2]Department of Biomedical Sciences, College of Veterinary Medicine, Iowa State University, Ames, IA 50011, USA

*Correspondence to: Jinoh Kim, 2086 Vet Med, 1800 Christensen Drive, Iowa State University, Ames, IA 50010, Email: jinohk@iastate.edu, Tel: 515-294-3401

Key words: ATF6, BTB, collagen, COPII, CUL3, IRE1α, nemaline myopathy, PERK, unfolded protein response

ABSTRACT

CUL3-RING ubiquitin ligases (CRL3s) are involved in diverse cellular processes through over two hundred BTB-domain proteins. KLHL12, a BTB-domain protein, has been suggested to play an essential role in export of unusually large cargo molecules like procollagen from the endoplasmic reticulum (ER). It has been suggested that $CRL3^{KLHL12}$ mono-ubiquitinates SEC31 and mono-ubiquitinated SEC31 increases the dimension of a COPII coat to accommodate the large cargo molecules. As we examined this model, we found that functional $CRL3^{KLHL12}$ was indeed critical for the assembly of large COPII structures. However, it did not directly affect collagen secretion, but instead influenced collagen synthesis in human skin fibroblasts (HSFs). These results also suggest that there is a $CRL3^{KLHL12}$–independent collagen secretion route. Unexpectedly, $CRL3^{KLHL12}$ strongly influenced the levels of sensors of the unfolded protein response (UPR) such as PERK and IRE1α. Interestingly, different cell lines reacted differently to CUL3 depletion. This cell-line dependency appears to rely on a cell-line specific BTB-domain protein(s) and a cell-line specific substrate(s) of the BTB-domain protein. Consistent with this idea, depletion of a muscle-specific BTB-domain protein KLHL41 recapitulated the effects of CUL3 depletion in C2C12 myotubes. Based on these results we propose that $CRL3^{KLHL12}$ and $CRL3^{KLHL41}$ are regulators of the UPR sensors.

INTRODUCTION

Cullin-RING ubiquitin (Ub) ligases (CRLs) are the major E3 ligase family in eukaryotes[1]. A CRL is composed of a catalytic module and a substrate-specific adaptor module[1]. In CRL3s, CUL3 and RBX1 serve as the catalytic module and a BTB domain protein serves as the substrate-specific adaptor module[2-4]. There are 204 BTB domain genes in the human genome[5], predicting that CRL3s are involved in various cellular processes. Indeed, recent studies have shown that CRL3s are important regulators of different cellular and developmental processes such as mitosis, cytokinesis, cell death, gene expression control, Hedgehog signaling, WNT signaling and so on (see Genschik et al. for review[6]). Defects of CRL3s have been implicated in metabolic diseases, dystrophies, and cancers[6].

KLHL12 is a BTB domain protein and $CRL3^{KLHL12}$ plays an important role in export of procollagen from the endoplasmic reticulum (ER) by ubiquitinating SEC31, a component of a COPII coat[7,8]. The COPII coat consisting of SAR1, SEC23/SEC24 complex, and SEC13/SEC31 complex is able to generate transport vesicles at the ER exit sites that can package most soluble and membrane proteins destined to various cellular locations. Collagens are the major component of the extracellular matrix (ECM). Type I and II procollagens form about 300 nm-long rigid triple helices[9,10] and require COPII proteins for export from the ER[11-17]. Because COPII proteins typically generate vesicles limited to 60-80 nm in diameter, a mechanism must exist that allows COPII coat proteins to accommodate such large cargo molecules. When KLHL12 was overexpressed, larger COPII-coated vesicles (>500 nm) were observed[7] and collagens were found in large structures coated with SEC31 and KLHL12[18]. Furthermore, large COPII structures were generated even in the presence of lysine-free ubiquitin which prevents poly-ubiquitination of SEC31[7]. Based on these results, it was proposed that mono-ubiquitinated

SEC31 molecules contribute to enlargement of COPII vesicles and packaging of procollagen into the enlarged vesicles.

Despite the evidence for the role of KLHL12 in collagen secretion, there remains a gap in our understanding of CRL3s in regulation of collagen secretion. For example, although depletion of CUL3 profoundly disrupted a collagen deposition in the ECM in mouse embryonic stem (ES) cells, depletion of KLHL12 alone did not[7]. In contrast, depletion of COPII or TANGO-1 displays a profound effect on collagen deposition in the ECM or medium[19-21]. Thus, it is plausible that other BTB domain proteins also mediate the effect of CUL3 on collagen secretion or alternative secretion routes exist for collagen in different cells and tissues. As we investigated the proposed role of CUL3-KLHL12 in collagen secretion, we discovered new functions of CUL3-KLHL12 in collagen synthesis as well as in the unfolded protein response (UPR) of the ER.

RESULTS

MLN4924 is a potent inhibitor of CRL3s

The catalytic activity of $CRL3^{KLHL12}$ has been shown to be critical for assembly of large COPII vesicles and collagen export from the ER[7]. To modulate the activity of $CRL3^{KLHL12}$, we searched for small molecules that can inhibit the Ub ligase activity of $CRL3^{KLHL12}$. Cullin itself is not a catalytic enzyme, but a scaffold protein. The Ub ligase activity of CRL3 is activated by neddylation of CUL3 as CUL3 neddylation induces a drastic conformational change near the RBX1 binding region[22]. This conformational change results in juxtaposition of E2-Ub to a substrate[23,24]. MLN4924 is a potent inhibitor of NEDD8-activating enzyme, resulting in strong inhibition of the catalytic activity of CRLs[25]. We used this small molecule to survey its effect on the catalytic activity of CRL3 and the interactions among the constituents of $CRL3^{KLHL12}$. For this purpose, we established a doxycycline-inducible HEK cell line stably expressing FLAG tagged KLHL12 (KLHL12-FLAG). Interestingly, MLN4924 treatment not only prevented CUL3 neddylation (Fig. 1A), but also stabilized KLHL12 (Fig. 1A, Input; Fig. S3, WT). This result suggests that turnover of KLHL12 is regulated by neddylation of CRLs. When we immunoprecipitated KLHL12, similar levels of SEC31 or CUL3 were co-precipitated regardless of inhibitor treatment (Fig. 1A, IP). Although apparent levels of SEC31 and CUL3 bound to KLHL12 were not affected by MLN4924 treatment, there seemed to be a decrease in the relative amounts of SEC31 bound to KLHL12 as there were more KLHL12 molecules due to stabilization. Thus, neddylation of CUL3 seems to help form $CRL3^{KLHL12}$-SEC31 complex more effectively.

We then asked whether MLN4924 inhibits the catalytic activity of CRL3s. Unfortunately, however, ubiquitinated forms of endogenous SEC31 were not detected under our experimental

conditions. To circumvent this problem, we took advantage of the observation that turnover of KLHL12 is stabilized by MLN4924 (Fig. 1A). It has been reported that an overactive form of CUL3 degrades KLHL3 by facilitating KLHL3 poly-ubiquitination and MLN4924 stabilizes KLHL3 by inhibiting CUL3-dependent KLHL3 poly-ubiquitination[26]. In analogy, KLHL12 may be ubiquitinated by CUL3. If this is the case, MLN4924 would inhibit KLHL12 ubiquitination. Indeed, MLN4924 treatments inhibited ubiquitination of KLHL12 (Fig. 1B), consistent with the idea that CUL3 ubiquitinates KLHL12. To corroborate this idea, we generated KLHL12 constructs with mutations at the KLHL12-CUL3 interface (Fig. S1 and Table S1, Mut B was not expressed for unknown reasons). Mut A or Mut C showed defects in CUL3 binding (Fig. S2A, B). They were also ubiquitinated with reduced efficiency (Fig. 1C). Our results indicate that KLHL12 ubiquitination is CUL3-dependent. Taken together, our data suggest that MLN4924 is a potent inhibitor of $CRL3^{KLHL12}$.

Interestingly, we noticed a strong reduction of neddylated (ned)-CUL3 bound to Mut A or Mut C when evaluated by immunoprecipitation (Fig. S2B). This was not due to lack of ned-CUL3 as we observed ned-CUL3 in total cell lysates prepared from cells stably expressing the KLHL12 constructs (Fig. S3). Thus, our data suggest that Mut A and Mut C do not form stable ned-CUL3-KLHL12 complexes. Mut A and Mut C also showed defects in KLHL12-SEC31 interaction (Fig. S2C, D). Clearly, the KLHL12-CUL3 interface is important not only for KLHL12-CUL3 interaction, but also for KLHL12-SEC31 interaction. Because ned-CUL3 species were deficient in mutant KLHL12-CUL3 complexes, this lack of ned-CUL3 in the complex likely contributed to the defective SEC31 binding. A similar finding was observed with KLHL12-SEC31 interaction in the presence of MLN4924 (Fig. 1). Note that although apparent levels of SEC31 and CUL3 bound to KLHL12 were not affected by MLN4924 treatment, there

was a decrease in the relative amounts of SEC31 bound to KLHL12 due to KLHL12 stabilization.

Formation of large COPII structures relies on functional CRL3^{KLHL12}

Because MLN4924 prevents neddylation of CUL3, an essential step for the activity of CRLs, we asked whether this inhibitor blocks the formation of large COPII-coated structures. To test this possibility, we treated the 293 cells stably expressing KLHL12 with MLN4924 and monitored COPII-KLHL12-coated structures via immunofluorescent microscopy. As previously reported, overexpression of KLHL12 induced formation of large COPII-KLHL12-coated structures (Fig. 2A, DMSO panel). In the presence of MNL4924, we observed aberrant COPII-KLHL12 structures with reduced SEC31 signals (Fig. 2A, MLN4924 panels), suggesting that the catalytic activity of CRL3^{KLHL12} is necessary for formation of large COPII coats.

We also monitored large COPII structures induced by expression of Mut A or Mut C (Fig. 2B). Interestingly, Mut A induced formation of apparently normal COPII-KLHL12 structures except that intensities of SEC31 fluorescence were slightly weaker than those of WT (Fig. 2B). Mut C induced formation of elongated COPII-KLHL12 structures with strongly reduced SEC31 fluorescence. These results reflect reduced interactions between the mutant KLHL12s and SEC31 (Fig. S2C, D). Taken together with the MLN4924 results, our data suggest that a proper KLHL12-CUL3 interaction and CUL3 neddylation are important for formation of large COPII-KLHL12 structures.

MLN4924 reduces intracellular levels of, but not secretion of collagen

Since MLN4924 treatment induced the formation of aberrant structures, we expected that this inhibitor reduces collagen secretion. We used human dermal fibroblasts (HSFs) which secrete type I collagen robustly because the 293 cells do not express type I collagen (Fig. S4). Intracellular collagen molecules were efficiently depleted within 3h in HSFs when new collagen synthesis was blocked (Fig. 3A). MLN4924 treatment inactivated CRL3s as indicated by the absence of ned-CUL3 (Fig. 3B, see the CUL3 panel). Unexpectedly, however, secretion of collagen was not affected by MLN4924 treatments (Fig. 3B and C), but the levels of intracellular collagen were reduced by the inhibitor treatments (Fig. 3B and D). Although the deposition of collagen in the medium was not attenuated despite the reduction of intracellular collagen levels by 24h, prolonged inhibitor treatments (> 24h) eventually blocked additional deposition of collagen in the medium (Fig. S5, see 48h and 72h). This was due to complete absence of collagen in the cells. These data suggest that CRLs primarily regulate cellular collagen levels. While our data gave us an interesting clue toward a new role of CUL3 in collagen, we did recognize that MLN4924 influences different CRLs and may also interact with unknown targets.

CUL3 is a regulator of collagen synthesis

To test if CUL3 is indeed responsible for regulation of collagen levels we used an approach of RNA interference (RNAi) with small interfering RNAs (siRNAs) (Fig. 4A, B). Initially, we performed RNAi in the absence of fetal bovine serum during the transfection step (16 h) where cells were exposed to transfection reagents. Subsequently, we realized that inclusion of the serum during this step yielded more robust results. When the serum was present during the transfection step, intracellular collagen levels increased (Fig. 4A, C)(compare lane 1 with lane 3; lane 2 with lane 4). This result is consistent with previous reports that the serum enhances

synthesis of type I collagen in HSFs[27,28]. Depletion of CUL3 enhanced the levels of intracellular and secreted collagen especially when the serum was present (Fig. 4A, C, D)(compare lane 3 with lane 4). This was unexpected because the MLN4924 treatment reduced collagen levels. However, considering the inhibitory activity of MLN4924 on the NEDD8-activating enzyme and diverse cellular processes governed by the NEDD8-activating enzyme, we concluded that CUL3 RNAi is more specific than the MLN4924 treatment.

The increase in levels of secreted and intracellular collagen suggests that collagen gene expression is increased by CUL3 depletion. To test this possibility, we measured levels of *COL1A1* mRNAs with a real time quantitative PCR (RT-qPCR) (Fig. 4E). As expected, we observed about 7-fold increase in the levels of COL1A1 mRNAs by CUL3 depletion. These results indicated that CUL3 regulates synthesis of COL1A1.

CUL3 is a regulator of the unfolded protein response (UPR) of the ER

It was intriguing that the effect of CUL3 RNAi on collagen became significant when the serum was present and that the effect of CUL3 RNAi on collagen was lost when the serum is absent. Serum provides cells with growth factors that stimulate collagen synthesis[29]. It has been also reported that a serum deprivation can induce ER stress (i.e., the UPR), which leads to inhibition of collagen synthesis in HSFs[30]. However, because we added back the serum after the transfection step and continued to incubate the cells in a serum containing medium for 48h, ER stress triggered by the serum withdrawal would be limited. Nevertheless, we tested whether our serum withdrawal procedure could trigger ER stress, masking the effect of CUL3 RNAi on collagen. For this purpose, we monitored changes in the levels of the UPR sensors such as PERK, IRE1α, and ATF6α[31]. Remarkably, CUL3 RNAi led to an increase in the levels of PERK

and IRE1α, but not those of full-length (FL) ATF6α. (Fig. 4A, F, G). Note that ATF6α FL is transported from the ER to the Golgi where it is processed to the N-terminal fragment (NTF) when the UPR is activated[32]. Phosphorylation of eIF2α, a downstream molecule of the PERK signaling pathway[33], was enhanced by CUL3 RNAi (Fi.g 4A, H). This enhancement became quite significant when the serum was present. However, when serum was absent, phosphorylation of eIF2α was not enhanced by CUL3 RNAi with strong statistical significance even though the levels of PERK and IRE1α were increased. Perhaps this was due to a low signal to noise ratio of p-eIF2α under the condition. However, it was clear that our serum withdrawal procedure did not trigger ER stress by itself (Fig. 4, compare lane 1 with lane 3 for PERK, IRE1α, p-eIF2α, and ATF6α). It should be noted that phosphorylation of eIF2α was enhanced by CUL3 RNAi even in the absence of extrinsic ER stressors such as DTT, thapsigargin, and tunicamycin. These results suggest that CUL3 modulates levels of UPR sensors such as PERK and IRE1α and that CUL3 regulates PERK signaling.

We then asked whether the increase in the amounts of PERK and IRE1α leads to an overactivation of the UPR when cells are stressed with an extrinsic ER stressor. For this purpose, we treated HSFs with DTT (Fig. 5). DTT treatments retarded the mobility of PERK and IRE1α in SDS-PAGE (Fig. 5A). These shifts in mobility have been shown to be caused by phosphorylation[34]. The levels of PERK and IRE1α species including the slowly migrating ones were increased by CUL3 RNAi upon DTT treatments, but not those of ATF6α-FL, suggesting that UPR signaling branches involving PERK and IRE1α are upregulated (Fig. 5 A, C-E). We also monitored changes in downstream components of the UPR. Although phosphorylation of eIF2α was enhanced by CUL3 RNAi alone, the DTT treatments did not further enhance

phosphorylation of eIF2α (Fig. 5A, F). XBP1 is a critical component of the IRE1α pathway and a UPR induction triggers synthesis of the spliced form of XBP1[35,36]. The DTT treatments induced synthesis of spliced XBP1 as expected (Fig. 5A). CUL3 RNAi combined with DTT treatments led to a significant increase of spliced XBP1 compared to the DTT treatments alone (Fig. 5A, G). CUL3 depletion did not change the levels of ATF6α-NTF (Fig. 5A, H). Based on these observations we concluded the CUL3 is also an important regulator of IRE1α signaling in HSFs.

There are 204 BTB domain genes which likely serve as a substrate-specific adaptor for CUL3 in the human genome[5]. Different cell lines/tissues are expected to have different profiles of BTB-domain proteins. Thus, we asked if the newly found CUL3-UPR link is observed in different cell types. To address this question we performed RNAi in IMR90 and HeLa (Fig. 6). The effects of CUL3 depletion on IRE1α and PERK were observed in IMR90 (Fig. 6 A and B). Interestingly, CUL3 RNAi increased levels of PERK but not those of IRE1α in HeLa cells (Fig. 6A and C), indicating that CUL3 does not always regulate levels of PERK and IRE1α concurrently. Our results are consistent with the idea that CUL3 regulates the levels of PERK and IRE1α with at least two different BTB domain proteins that are differentially expressed in HSFs, IMR90, and HeLa (Fig. 6D).

KLHL12 regulates collagen levels and the UPR

We then tested whether the effects of CUL3 on collagen and the UPR is mediated through KLHL12 in HSFs. KLHL12 RNAi led to a reduction of secreted as well as intracellular collagen (Fig. 7A-D). It is intriguing that CUL3 depletion and KLHL12 depletion resulted in opposite

outcomes with respect to collagen synthesis. This result suggests a complexity in regulation of collagen synthesis by CUL3 and its adaptors. Regardless, KLHL12 does not influence collagen secretion directly, rather does so probably by affecting collagen synthesis. Interestingly, KLHL12 RNAi led to an increase in the levels of PERK and IRE1α when the serum was present during transfection, but not when the serum was absent during transfection (Fig. 7A, E, F). We believe this is partly due to inefficiency of KLHL RNAi under the condition (Fig. 7B). Thus, we identified a new function of $CRL3^{KLHL12}$ that it regulates the levels of collagen and UPR sensors.

CUL3 and a muscle-specific BTB domain protein regulate PERK levels

While we examined the effect of CUL3 depletion in various cell types, we noticed that PERK levels were reduced by CUL3 depletion in C2C12 mouse myotubes (CMTs) (Fig. 8). Levels of IRE1α were not affected by CUL3 RNAi. This response is likely due to myotube-specific BTB domain proteins. As an effort to identify such BTB-domain proteins, we took advantage of the observations that KLHL41 is the most abundant BTB-domain protein in CMTs[37], it is a muscle-specific protein[38], and it interacts with CUL3[39]. Depletion of KLHL41 resulted in similar responses to depletion of CUL3 (Fig. 8), supporting the notion that the muscle-specific effect of CUL3 on the UPR is conveyed through the muscle-specific BTB domain protein KLHL41. Based on these results we conclude that $CRL3^{KLHL41}$ is a regulator of PERK in muscle cells.

DISCUSSION

Our data support the idea that the integrity of $CRL3^{KLHL12}$ is critical for formation of KLHL12-COPII-coated structures as MLN4924 treatments or KLHL12 mutants compromised KLHL12-COPII structures. Surprisingly, depletion of CUL3 or KLHL12 affected collagen levels in the cell as well as in the culture medium when the siRNA transfection was performed in the presence of the serum in HSFs. However, similar depletion did not influence secretion, nor intracellular levels of collagen when the siRNA transfection was performed in the absence of the serum. Although the physiological relevance of these two *in vitro* conditions remains to be determined, a quantitative proteomic study has revealed that levels of COL2A1 and COL9A1 are enhanced in skeletal muscles of skeletal muscle-specific *CUL3* knockout mice[40]. Apparently, CUL3 plays a role in regulating collagen synthesis and there seems to exist a CUL3/KLHL12-independent collagen secretion pathway *in vitro* and *in vivo*. Thus, these results are inconsistent with the model that $CRL3^{KLHL12}$ is essential for collagen export. However, our data do not exclude a possibility that there is a $CRL3^{KLHL12}$–dependent collagen secretion pathway under a specific condition (i.e., early embryonic development). Perhaps, multiple mechanisms are present to export collagen from the ER.

One of the salient aspects of our findings is that CUL3 regulates the UPR. Because of the enhanced levels of PERK and IRE1α due to CUL3 depletion in HSFs, downstream UPR signaling was activated accordingly, indicating that CUL3 regulates UPR signaling. Although the effect of CUL3 on collagen synthesis was influenced by the serum, the effect of CUL3 on the UPR sensors was not affected by the serum. These results suggest that the CUL3-UPR interaction is independent of the serum-induced ER stress.

CUL3 depletion led to about 2-fold increase of COL1A1 proteins and about 7-fold increase of *COL1A1* mRNAs. These results suggest that there is a translational block under this condition. Perhaps enhanced PERK-eIF2α signaling induced by CUL3 depletion accounts for this inhibitory effect because it is well established that p-eIF2α inhibits translation of mRNA into protein[33].

If CUL3 triggered ER stress in a similar way to an ER stressor like DTT, tunicamycin, and thapsigargin, we would have observed an activation of all three signaling routes of the UPR. However, ATF6α levels and its proteolytic processing were not affected by CUL3 depletion. Thus, we do not think CUL3 depletion works in a similar way to the ER stressors. In addition, those ER stressors do not alter the levels of the UPR sensors, but instead shift the molecular weight (band smearing due to phosphorylation) (Fig. 5A, compare lane 1 with lane 2 or lane 3 for PERK and IRE1α). Our results are consistent with the idea that CUL3 influences the UPR specifically (i.e., PERK and IRE1α). This specific effect likely involves a specific BTB domain protein(s) and its cell line-specific substrate molecule (i.e., a transcription activator or a repressor). Although we have not found a cell line where CUL3 regulates ATF6, it is formally possible that CUL3 regulates ATF6 in a certain cell line.

KEAP1, a BTB-domain protein, regulates UPR signaling involving NRF2[41]. NRF2 is a transcription factor which regulates the expression of antioxidant genes in response to oxidative stress[42,43]. NRF2 levels are maintained via association with KEAP1[44]. This association is regulated by PERK-dependent phosphorylation of NRF2[45]. This mode of UPR regulation by KEAP1 is distinct from the newly identified mode of UPR regulation by CUL3 where CUL3 regulates PERK and IRE1α. Thus, CUL3 and its adaptor molecules influence the UPR with multi-faceted strategies, emphasizing fundamental importance of CUL3 in UPR regulation.

We discovered that CUL3 regulates UPR sensors in a cell line-specific manner: 1) CUL3 depletion increased levels of PERK and IRE1α in HSF and IMR90, 2) CUL3 depletion increased levels of PERK, but not those of IRE1α in HeLa cells, and 3) CUL3 depletion reduced levels of PERK, but not those of IRE1α in CMTs. We believe that this cell-type specificity arises due to differentially expressed BTB-domain proteins and their substrate(s). CUL3 recognizes its substrate molecules through a BTB-domain protein[6]. Two hundreds and four BTB-domain genes are likely expressed in a tissue-specific manner in human cells[5]. In fact, KLHL41 is expressed exclusively in muscles[46]. The cellular phenotypes induced by depletion of KLHL41 were similar to those induced by depletion of CUL3 in CMTs, suggesting that the effect of CUL3 is relayed through KLHL41. In addition, a BTB-domain protein can recognize several different target molecules, vastly expanding functional roles of CUL3. Importance of tissue-specific expression of a substrate molecule(s) of KLHL41 was also obvious in our data. Mere absence of KLHL41 is not sufficient to lower the levels of PERK because PERK levels are relatively high in cell lines (i.e., HSFs) which do not express KLHL41. In addition, although KLHL41 is expressed much less in myoblasts than in myotubes, the levels of PERK are quite high in myoblasts compared to those in myotubes (Fig. 6S, compare day 0 to day 2-5). Thus, a myotube-specific substrate(s) of KLHL41 likely plays a critical role in PERK regulation. It is possible that this substrate molecule regulates PERK levels through a synthetic or a degradative mechanism. The identity of the substrate remains to be determined.

BTB-domain proteins are necessary for a proper muscle function. Mutations of *KLHL40*, *KLHL41*, and *KBTBD13* cause nemaline myopathy[47-49]. KLHL9 is associated with a distal myopathy in humans[50]. KLHL31 is linked to a congenital myopathy in mice[51]. Furthermore, muscle-specific deletion of *CUL3* disrupts muscle physiology profoundly, highlighting the

fundamental importance of CUL3 and its substrate-specific adaptor molecules in muscle functions[40]. Interestingly, a quantitative proteomic analysis of mice with a *TPM3* mutation showed about a 3-4 fold reduction of PERK (a.k.a. EIF2AK3) in the diaphragm muscles[52]. *TPM3* mutations also cause nemaline myopathy in humans[53]. Perhaps UPR dysregulation is common in a subset of nemaline myopathy and related congenital myopathies.

METHODS

Plasmid and siRNA

The pcDNA5/FRT/TO KLHL12-FLAG construct was a gift of Michael Rape's laboratory (University of California, Berkeley, CA, USA). The KLHL12 Mut A (ELSE65-68AAAA), Mut B (CLLQLK111-116AAAAAA), and Mut C (FAETHNC141-147AAAAAAA) were generated by site-directed mutagenesis (Fig. S1 and Table S1). pCMV6-Entry (PS100001), human pCMV6-KLHL40-Myc-DDK (RC213832), and human pCMV6-KLHL41-Myc-DDK (RC200295) were purchased from Origene (Rockville, MD, USA). The control (D-01910-10-50), human–specific CUL3 (M-010224-02), and KLHL12 siRNAs (M-015890-02), mouse-specific CUL3 (M-062951-01-0005), KLHL40 (M-016211-02-0005), and mouse-specific KLHL41 (M-045964-01-0005) were purchased from Dharmacon (Lafayette, CO, USA). Sequences of these siRNAs are shown as follows. Control (pool of 4) siRNAs: 5'-UAGCGACUAAACACAUCAA-3', 5'-UAAGGCUAUGAAGAGAUAC3', 5'-AUGUAUUGGCCUGUAUUAG-3', 5'-AUGAACGUGAAUUGCUCAA-3'. Human CUL3 (pool of 4) siRNAs: 5'- CCGAACAUCUCAUAAAUAA-3', 5'-GAGAAGAUGUACUAAAUUC-3', 5'-GAGAUCAAGUUGUACGUUA-3', 5'-GCGGAAAGGAGAAGUCGUA-3'. Mouse CUL3 (pool of 4) siRNAs: 5'-GAAAGUAGAAGCUAGGAUU-3', 5'- CGGCAAACUUUAUUGGAUA-3', 5'-GGUGAUGAUUAGAGACAUA-3', 5'- CCAAGUCCAGUUGUUAUUA-3'. Human KLHL12 (pool of 4) siRNAs : 5'-GGAAGGUGCCGGACUCGUA-3', 5'-GCGCUAUGAUCCAAACAUU-3', 5'-GAAGAAUCCUUGCCUAACC-3', 5'-UAAUCAAGUGCGACGAAAU-3'. Mouse KLHL40 (pool of 4) siRNAs: 5'-GCGCAUACUUCCUGCAGUU-3', 5'-GAACAAGAUGUGCGUCUAU-3', 5'-

CUACGUAAUUGGCGGCAAA-3', 5'-AUGAGGAGGCCGAACGUAU-3'. Mouse KLHL41 (pool of 4) siRNAs: 5'-GGGAAGUGAUGACGGAAUU-3', 5'-GUUCAUCAUUGCACCCUA-3', 5'-GGCAUGGAAUGUUUGUUAA-3', 5'-CCGGUUACCUGAACGAUAU-3'

Antibodies and chemicals

Rabbit anti-PC1 antibodies were a gift from L. Fisher (LF-68, 1:8000, National Institute of Dental and Craniofacial Research, Bethesda, MD, USA)[54]. Rabbit anti-ribophorin I antibody (1:5,000) was a gift from Schekman laboratory (University of California, Berkeley, CA, USA). Additional antibodies we used include rabbit anti-CUL3 (A301-109A, 1:1000, Bethyl Laboratories, Universal Biologicals, Cambridge, UK), mouse FK2 anti-Ub (BML-PW8810, 1: 1000, Enzo Life Sciences, Farmingdale, NY, USA), anti-FLAG (F3165, F7425, 1:1500, Sigma-Aldrich, St. Louis, MO, USA), mouse anti-KLHL12 (#30058, 1:1000, ProMab Biotechnology, Richmond, CA,USA), rabbit anti-KLHL40 (#HPA024463, 1:1000, Sigma-Aldrich, St. Louis, MO, USA), rabbit anti-KLHL41 (#AV38732, 1:1000, Sigma-Aldrich, St. Louis, MO, USA), mouse and rabbit anti-SEC31A (#612350, BD Biosciences, San Diego, CA, A302-336A, Bethyl Laboratories, Universal Biologicals, Cambridge, UK), rabbit anti-IRE1α (#3294), PERK (#5683), p-eIF2α (Ser51, #9721), total-eIF2α (#9722), XBP-1s (#12782) (1:1000 final dilution; all from Cell signaling Technology, Danvers, MA, USA), monoclonal anti-ATF6α antibody (73-500, 1:1200, B-Bridge International, Inc., Santa Clara, CA, USA), monoclonal anti-α-tubulin (TU-02, sc-8035, 1:2000, Santa Cruz Biotechnology, Dallas, TX, USA). Hygromycin B (10687-010) and blasticidin S (R210-01) were purchased from Invitrogen (Carlsbad, CA, USA). Cycloheximide (CHX, C4859), dimethyl sulfoxide (DMSO, D4540,) and 1, 4-dithiothreitol

(DTT, D0632) were purchased from Sigma-Aldrich (St. Louis, MO, USA). Protease inhibitor cocktail (Mannheim, Germany), MLN4924 (15217, Cayman Chemical, Ann Arbor, MI, USA), MG132 (474790, Calbiochem, San Diego, CA, USA), brefeldin A (BFA, #9972, Cell signaling Technology, Danvers, MA, USA) were also used.

Cell culture and transfection

Normal human foreskin fibroblasts (CRL-2091), HeLa cells (HeLa, CCL-2), human lung fibroblasts (IMR-90, CCL-186), and mouse C2C12 myoblasts (CRL1772) were purchased from the American Type Culture Collection (ATCC, Manassas, VA, USA). Cells were maintained in low-glucose Dulbecco's Modified Eagle Medium (DMEM) with 10% fetal bovine serum (FBS) and 1% penicillin–streptomycin. Flp_In T-REx^{TM} 293 host cell line containing a stably integrated FRT site and tetracycline (Tet) repressor was grown in high-glucose DMEM, supplemented with 10% FBS, blasticidin and hygromycin B as instructed by the manufacturer (Gibco/Thermo Fisher, Waltham, MA, USA) and gene expression was induced by 1 μg/ml doxycycline. Cells were maintained in high-glucose Dulbecco's Modified Eagle Medium (DMEM) with 10% fetal bovine serum (FBS) and 1% penicillin–streptomycin for proliferation (Gibco/Thermo Fisher, Waltham, MA, USA). Differentiation C2C12 myoblasts into myotubes was initiated by incubating the cells in high-glucose Dulbecco's Modified Eagle Medium (DMEM) with 2 % Horse serum (HS) (Thermo Fisher, Waltham, MA, USA) and 1% penicillin-streptomycin[55]. Cell lines were maintained in a water jacketed incubator at 37°C with 5% CO_2 enrichment. Lipofectamine LTX 3000 was used for plasmid DNAs transfection and Lipofectamine RNAiMAX for siRNAs transfection according to the manufacturer's protocols

unless specified otherwise. All of the cell culture and transfection reagents were purchased from Invitrogen (Carlsbad, CA, USA).

Establishing stable cell lines

Flp-In™ T-REx™ 293 cells stably expressing Tet-inducible KLHL12 WT, Mut A, and Mut C were generated according to the manufacturer's instructions (Flp-In™ System, Invitrogen, Carlsbad, CA, USA). Briefly, the Flp-In™ T-REx™ 293 Cells (R780-07) were plated onto 6-well plates and incubated for 24 h. The following day, the cells were transfected using 5 μl Lipofectamine LTX with 0.5 μg of a KLHL12 construct and 1.0 μg of pOG44 (V6005-20). After 48 h post-transfection, the cells were replated on 24-well plates and subjected to selection with hygromycin B (100 μg/ml) and blasticidin S (10 μg/ml) for up to 4 weeks and *KLHL12* expression was induced by 1 μg/ml doxycycline.

Co-immunoprecipitation and Immunoblotting

For co-immunoprecipiation, cells were collected by centrifugation and lysed by douncing 30 times using buffer A (0.1% NP-40, 2.6 mM KCl, 1.5 mM KH_2PO_4, 140 mM NaCl, 8 mM Na_2HPO_4-$7H_2O$, and 1X protease inhibitor cocktail) on ice. After centrifugation for 15 min at 14,000 rpm at 4°C, cleared lysates were incubated with indicated antibodies overnight in the cold room, followed by incubation with protein A or protein G Sepharose beads (GE Healthcare, Milwaukee, WI, USA) for 3 h with gentle rocking in the cold room. The beads were harvested by centrifugation and washed three times with buffer A. After adding the SDS-sample buffer and

heating for 5 min at 95 °C, proteins were resolved with SDA-PAGE and processed for immunoblotting.

For routine immunoblotting analysis, cells were lysed with buffer B (20 mM Tris-HCl, pH 7.5, 150 mM NaCl, 1 mM Na_2EDTA, 1 mM EGTA, 1% NP-40, 1% sodium deoxycholate, 2.5 mM sodium pyrophosphate, 1 mM β-glycerophosphate, 1 mM Na_3VO_4, 1X complete protease inhibitor cocktail) on ice for 15 minutes. Cell lysates were cleared by centrifugation at 14,000 rpm for 15 minutes at 4°C. Cleared lysates were quantified using Pierce BCA Protein Assay Kit (Thermo Fisher Scientific, Waltham, MA, USA). Equal amounts of proteins were resolved on 6 or 10% SDS-PAGE, transferred to PVDF membrane (Millipore, Bedford, MA, USA), probed with primary antibodies, subsequently with horseradish peroxidase-conjugated secondary antibodies, and visualized with ECL Prime (GE Healthcare, Pittsburgh, PA, USA). Band intensity was quantified using the ImageJ software. Protein levels were normalized to ribophorin I or α-tubulin and are presented as mean ± standard deviation.

Ubiquitination assay

The ubiquitination assay was performed as previously described[56]. Briefly, Tet-inducible KLHL12-FLAG-expressing 293 cells were treated with MG132 for 24 h prior to harvest. To assess endogenous ubiquitination of KLHL12, cells were harvested in PBS containing 5 mM NEM and lysed in 1% SDS by boiling for 10 min. Cell lysates were diluted to 0.1% SDS by adding lysis buffer (6 M guanidinium-HCl buffer (pH 8.0)) containing protease inhibitors and 5 mM NEM, and immunoprecipitated with anti-FLAG antibody followed by immunoblot.

Immunofluorescent microscopy

Cells were plated in 6-well plate with acid-washed glass coverslips. After 24h, cells were fixed with 4% paraformaldehyde (PFA) in DPBS for 30 min, washed five times with PBS and permeabilized with 0.1% Triton X-100 in DPBS for 15 min at room temperature. Primary antibodies were used in 0.5% BSA in DPBS. Cells were incubated with blocking buffer (0.5% BSA in PBS) for 30 min at RT followed by 1 h incubation at RT with rabbit anti-FLAG antibody (1:500, Sigma-Aldrich, St. Louis, MO, USA) and mouse anti-SEC31A antibody (1:500, BD Biosciences, NJ, USA) and then secondary antibodies such as Alexa Fluor 488 goat anti-rabbit IgG and Alexa Fluor 594 goat anti-mouse IgG (1:500, Molecular Probes, Invitrogen, Carlsbad, CA, USA). Antibody incubations were followed by five PBS washes. Images were obtained using a confocal laser microscopy (Nikon C1, Nikon, Tokyo, Japan), and merges of images were processed using Nikon EZ-C1 viewer software.

Real-time quantitative PCR with reverse transcription

RNA was obtained from fibroblast cells using Trizol reagent (Invitrogen, Carlsbad, CA, USA) according to the manufacturer's instructions. Complementary DNAs (cDNAs) were synthesized from total RNA using Superscript II First-strand Synthesis kit (Invitrogen, Carlsbad, CA, USA) and quantified by real-time PCR using the IQ SYBR green supermix kit (Bio-Rad Laboratories, Hercules, CA, USA) and the following primers: human *COL1A1*, 5'-GTGTTGTGCGSTGSCG-3' and 5'-TCGGTGGGTGACTCT-3'; human *CUL3*, 5'-CTGGTGTATCTTTAGGTGGTG-3' and 5'-GTGCTGGTGGGATGTTG-3'; human *GAPDH*, 5'-CTCCTCCACCTTTGACGC-3' and

5'-CCACCACCCTGTTGCTGT-3'. Gene expression levels were normalized to *GAPDH* expression levels.

Statistical analysis

Statistical analyses were performed using GraphPad Prism (GraphPad Software Inc., La Jolla, CA, USA). The results of multiple experiments were presented with mean ± standard deviation (SD). P-values of less than 0.05 were considered statistically significant.

ACKNOWLEDGEMENTSs

Research reported in this publication was supported by the National Institute of General Medical Sciences of the National Institutes of Health under award number R01GM110373.

AUTHOR CONTRIBUTIONS

K.K., S.P., J.K. designed the study; K.K., S.P. collected the data; K.K, J.K wrote the article and all contributed to editing and reviewing the submission.

COMPETING INTERESTS

The authors declare no competing interests.

REFERENCES

1 Petroski, M. D. & Deshaies, R. J. Function and regulation of cullin-RING ubiquitin ligases. *Nat Rev Mol Cell Biol* **6**, 9-20, doi:10.1038/nrm1547 (2005).

2 Furukawa, M., He, Y. J., Borchers, C. & Xiong, Y. Targeting of protein ubiquitination by BTB-Cullin 3-Roc1 ubiquitin ligases. *Nat Cell Biol* **5**, 1001-1007, doi:10.1038/ncb1056 (2003).

3 Xu, L. *et al.* BTB proteins are substrate-specific adaptors in an SCF-like modular ubiquitin ligase containing CUL-3. *Nature* **425**, 316-321, doi:10.1038/nature01985 (2003).

4 Pintard, L. *et al.* The BTB protein MEL-26 is a substrate-specific adaptor of the CUL-3 ubiquitin-ligase. *Nature* **425**, 311-316, doi:10.1038/nature01959 (2003).

5 Stogios, P. J. & Prive, G. G. The BACK domain in BTB-kelch proteins. *Trends Biochem Sci* **29**, 634-637, doi:10.1016/j.tibs.2004.10.003 (2004).

6 Genschik, P., Sumara, I. & Lechner, E. The emerging family of CULLIN3-RING ubiquitin ligases (CRL3s): cellular functions and disease implications. *EMBO J* **32**, 2307-2320, doi:10.1038/emboj.2013.173 (2013).

7 Jin, L. *et al.* Ubiquitin-dependent regulation of COPII coat size and function. *Nature* **482**, 495-500, doi:nature10822 [pii]

10.1038/nature10822 (2012).

8 McGourty, C. A. *et al.* Regulation of the CUL3 Ubiquitin Ligase by a Calcium-Dependent Co-adaptor. *Cell* **167**, 525-538 e514, doi:10.1016/j.cell.2016.09.026 (2016).

9 Bachinger, H. P., Morris, N. P. & Davis, J. M. Thermal stability and folding of the collagen triple helix and the effects of mutations in osteogenesis imperfecta on the triple helix of type I collagen. *Am J Med Genet* **45**, 152-162, doi:10.1002/ajmg.1320450204 (1993).

10 Bonfanti, L. *et al.* Procollagen traverses the Golgi stack without leaving the lumen of cisternae: evidence for cisternal maturation. *Cell* **95**, 993-1003, doi:S0092-8674(00)81723-7 [pii] (1998).

11 Ohisa, S., Inohaya, K., Takano, Y. & Kudo, A. sec24d encoding a component of COPII is essential for vertebra formation, revealed by the analysis of the medaka mutant, vbi. *Dev Biol* **342**, 85-95, doi:S0012-1606(10)00172-7 [pii]

10.1016/j.ydbio.2010.03.016 (2010).

12 Long, K. R. *et al.* Sar1 assembly regulates membrane constriction and ER export. *J Cell Biol* **190**, 115-128, doi:jcb.201004132 [pii]

10.1083/jcb.201004132 (2010).

13 Townley, A. K. *et al.* Efficient coupling of Sec23-Sec24 to Sec13-Sec31 drives COPII-dependent collagen secretion and is essential for normal craniofacial development. *J Cell Sci* **121**, 3025-3034, doi:jcs.031070 [pii]

10.1242/jcs.031070 (2008).

14 Boyadjiev, S. A. *et al.* Cranio-lenticulo-sutural dysplasia is caused by a SEC23A mutation leading to abnormal endoplasmic-reticulum-to-Golgi trafficking. *Nat Genet* **38**, 1192-1197, doi:ng1876 [pii]

10.1038/ng1876 (2006).

15 Garbes, L. *et al.* Mutations in SEC24D, encoding a component of the COPII machinery, cause a syndromic form of osteogenesis imperfecta. *Am J Hum Genet* **96**, 432-439, doi:10.1016/j.ajhg.2015.01.002 (2015).

16 Zhu, M. *et al.* Neural tube opening and abnormal extraembryonic membrane development in SEC23A deficient mice. *Sci Rep* **5**, 15471, doi:10.1038/srep15471 (2015).

17 Sarmah, S. *et al.* Sec24D-dependent transport of extracellular matrix proteins is required for zebrafish skeletal morphogenesis. *PLoS One* **5**, e10367, doi:10.1371/journal.pone.0010367 (2010).

18 Gorur, A. *et al.* COPII-coated membranes function as transport carriers of intracellular procollagen I. *J Cell Biol* **216**, 1745-1759, doi:10.1083/jcb.201702135 (2017).

19 Saito, K. *et al.* TANGO1 facilitates cargo loading at endoplasmic reticulum exit sites. *Cell* **136**, 891-902, doi:S0092-8674(08)01630-9 [pii]

10.1016/j.cell.2008.12.025 (2009).

20 Santos, A. J., Nogueira, C., Ortega-Bellido, M. & Malhotra, V. TANGO1 and Mia2/cTAGE5 (TALI) cooperate to export bulky pre-chylomicrons/VLDLs from the endoplasmic reticulum. *J Cell Biol* **213**, 343-354, doi:10.1083/jcb.201603072 (2016).

21 Jones, B. *et al.* Mutations in a Sar1 GTPase of COPII vesicles are associated with lipid absorption disorders. *Nat Genet* **34**, 29-31, doi:10.1038/ng1145

ng1145 [pii] (2003).

22 Merlet, J., Burger, J., Gomes, J. E. & Pintard, L. Regulation of cullin-RING E3 ubiquitin-ligases by neddylation and dimerization. *Cell Mol Life Sci* **66**, 1924-1938, doi:10.1007/s00018-009-8712-7 (2009).

23 Saha, A. & Deshaies, R. J. Multimodal activation of the ubiquitin ligase SCF by Nedd8 conjugation. *Mol Cell* **32**, 21-31, doi:10.1016/j.molcel.2008.08.021 (2008).

24 Petroski, M. D. & Deshaies, R. J. Mechanism of lysine 48-linked ubiquitin-chain synthesis by the cullin-RING ubiquitin-ligase complex SCF-Cdc34. *Cell* **123**, 1107-1120, doi:10.1016/j.cell.2005.09.033 (2005).

25 Soucy, T. A. *et al.* An inhibitor of NEDD8-activating enzyme as a new approach to treat cancer. *Nature* **458**, 732-736, doi:10.1038/nature07884 (2009).

26 McCormick, J. A. *et al.* Hyperkalemic hypertension-associated cullin 3 promotes WNK signaling by degrading KLHL3. *J Clin Invest* **124**, 4723-4736, doi:10.1172/JCI76126 (2014).

27 Freiberger, H., Grove, D., Sivarajah, A. & Pinnell, S. R. Procollagen I synthesis in human skin fibroblasts: effect on culture conditions on biosynthesis. *J Invest Dermatol* **75**, 425-430 (1980).

28 Murad, S., Tajima, S., Johnson, G. R., Sivarajah, S. & Pinnell, S. R. Collagen synthesis in cultured human skin fibroblasts: effect of ascorbic acid and its analogs. *J Invest Dermatol* **81**, 158-162 (1983).

29 Boraldi, F., Annovi, G., Paolinelli-Devincenzi, C., Tiozzo, R. & Quaglino, D. The effect of serum withdrawal on the protein profile of quiescent human dermal fibroblasts in primary cell culture. *Proteomics* **8**, 66-82, doi:10.1002/pmic.200700833 (2008).

30 Vonk, L. A. *et al.* Endoplasmic reticulum stress inhibits collagen synthesis independent of collagen-modifying enzymes in different chondrocyte populations and dermal fibroblasts. *Biochem Cell Biol* **88**, 539-552, doi:10.1139/o09-174 (2010).
31 Walter, P. & Ron, D. The unfolded protein response: from stress pathway to homeostatic regulation. *Science* **334**, 1081-1086, doi:10.1126/science.1209038 (2011).
32 Haze, K., Yoshida, H., Yanagi, H., Yura, T. & Mori, K. Mammalian transcription factor ATF6 is synthesized as a transmembrane protein and activated by proteolysis in response to endoplasmic reticulum stress. *Mol Biol Cell* **10**, 3787-3799, doi:10.1091/mbc.10.11.3787 (1999).
33 Harding, H. P., Zhang, Y. & Ron, D. Protein translation and folding are coupled by an endoplasmic-reticulum-resident kinase. *Nature* **397**, 271-274, doi:10.1038/16729 (1999).
34 DuRose, J. B., Tam, A. B. & Niwa, M. Intrinsic capacities of molecular sensors of the unfolded protein response to sense alternate forms of endoplasmic reticulum stress. *Mol Biol Cell* **17**, 3095-3107, doi:10.1091/mbc.E06-01-0055 (2006).
35 Calfon, M. *et al.* IRE1 couples endoplasmic reticulum load to secretory capacity by processing the XBP-1 mRNA. *Nature* **415**, 92-96, doi:10.1038/415092a (2002).
36 Yoshida, H., Matsui, T., Yamamoto, A., Okada, T. & Mori, K. XBP1 mRNA is induced by ATF6 and spliced by IRE1 in response to ER stress to produce a highly active transcription factor. *Cell* **107**, 881-891 (2001).
37 Deshmukh, A. S. *et al.* Deep proteomics of mouse skeletal muscle enables quantitation of protein isoforms, metabolic pathways, and transcription factors. *Mol Cell Proteomics* **14**, 841-853, doi:10.1074/mcp.M114.044222 (2015).
38 Taylor, A. *et al.* DNA sequence and muscle-specific expression of human sarcosin transcripts. *Mol Cell Biochem* **183**, 105-112 (1998).
39 Ramirez-Martinez, A. *et al.* KLHL41 stabilizes skeletal muscle sarcomeres by nonproteolytic ubiquitination. *Elife* **6**, doi:10.7554/eLife.26439 (2017).
40 Papizan, J. B., Vidal, A. H., Bezprozvannaya, S., Bassel-Duby, R. & Olson, E. N. Cullin-3-RING ubiquitin ligase activity is required for striated muscle function in mice. *J Biol Chem* **293**, 8802-8811, doi:10.1074/jbc.RA118.002104 (2018).
41 Cullinan, S. B., Gordan, J. D., Jin, J., Harper, J. W. & Diehl, J. A. The Keap1-BTB protein is an adaptor that bridges Nrf2 to a Cul3-based E3 ligase: oxidative stress sensing by a Cul3-Keap1 ligase. *Mol Cell Biol* **24**, 8477-8486, doi:10.1128/MCB.24.19.8477-8486.2004 (2004).
42 Chan, J. Y. & Kwong, M. Impaired expression of glutathione synthetic enzyme genes in mice with targeted deletion of the Nrf2 basic-leucine zipper protein. *Biochim Biophys Acta* **1517**, 19-26 (2000).
43 Chan, K. & Kan, Y. W. Nrf2 is essential for protection against acute pulmonary injury in mice. *Proc Natl Acad Sci U S A* **96**, 12731-12736 (1999).
44 Itoh, K. *et al.* Keap1 represses nuclear activation of antioxidant responsive elements by Nrf2 through binding to the amino-terminal Neh2 domain. *Genes Dev* **13**, 76-86 (1999).
45 Cullinan, S. B. *et al.* Nrf2 is a direct PERK substrate and effector of PERK-dependent cell survival. *Mol Cell Biol* **23**, 7198-7209 (2003).
46 du Puy, L. *et al.* Sarcosin (Krp1) in skeletal muscle differentiation: gene expression profiling and knockdown experiments. *Int J Dev Biol* **56**, 301-309, doi:10.1387/ijdb.113327lp (2012).

47 Sambuughin, N. *et al.* Dominant mutations in KBTBD13, a member of the BTB/Kelch family, cause nemaline myopathy with cores. *Am J Hum Genet* **87**, 842-847, doi:10.1016/j.ajhg.2010.10.020 (2010).

48 Ravenscroft, G. *et al.* Mutations in KLHL40 are a frequent cause of severe autosomal-recessive nemaline myopathy. *Am J Hum Genet* **93**, 6-18, doi:10.1016/j.ajhg.2013.05.004 (2013).

49 Gupta, V. A. *et al.* Identification of KLHL41 Mutations Implicates BTB-Kelch-Mediated Ubiquitination as an Alternate Pathway to Myofibrillar Disruption in Nemaline Myopathy. *Am J Hum Genet* **93**, 1108-1117, doi:10.1016/j.ajhg.2013.10.020 (2013).

50 Cirak, S. *et al.* Kelch-like homologue 9 mutation is associated with an early onset autosomal dominant distal myopathy. *Brain* **133**, 2123-2135, doi:10.1093/brain/awq108 (2010).

51 Papizan, J. B. *et al.* Deficiency in Kelch protein Klhl31 causes congenital myopathy in mice. *J Clin Invest* **127**, 3730-3740, doi:10.1172/JCI93445 (2017).

52 Sanoudou, D. *et al.* Skeletal muscle repair in a mouse model of nemaline myopathy. *Hum Mol Genet* **15**, 2603-2612, doi:10.1093/hmg/ddl186 (2006).

53 Laing, N. G. *et al.* A mutation in the alpha tropomyosin gene TPM3 associated with autosomal dominant nemaline myopathy. *Nat Genet* **9**, 75-79, doi:10.1038/ng0195-75 (1995).

54 Fisher, L. W., Stubbs, J. T., 3rd & Young, M. F. Antisera and cDNA probes to human and certain animal model bone matrix noncollagenous proteins. *Acta Orthop Scand Suppl* **266**, 61-65 (1995).

55 Miller, J. B. Myogenic programs of mouse muscle cell lines: expression of myosin heavy chain isoforms, MyoD1, and myogenin. *J Cell Biol* **111**, 1149-1159 (1990).

56 Xirodimas, D., Saville, M. K., Edling, C., Lane, D. P. & Lain, S. Different effects of p14ARF on the levels of ubiquitinated p53 and Mdm2 in vivo. *Oncogene* **20**, 4972-4983, doi:10.1038/sj.onc.1204656 (2001).

Figure legends

Figure 1. MLN4924, an inhibitor of NEDD8-activating enzyme, inhibits the activity of $CRL3^{KLHL12}$. (A and B) 293 cells stably expressing KLHL12-FLAG were incubated in the presence or absence of MLN4924. Expression of KLHL12-FLAG was induced with doxycycline. Cellular lysates were processed for immunoprecipitation using an anti-FLAG antibody. Closed arrowhead, neddylated CUL3; open arrowhead, unneddylated CUL3. *Nonspecific band. **Immunoglobulins. (C) An HA-tagged ubiquitin construct was expressed in HEK cells stably expressing wildtype (WT) or a mutant KLHL12 (Mut A or Mut C). Cellular lysates were processed for immunoprecipitation using an anti-FLAG antibody.

Figure 2. Aberrant large COPII structures with compromised $CRL3^{KLHL12}$. (A) 293 cells stably expressing WT KLHL12-FLAG were incubated in the presence (1μM) or absence (DMSO) of MLN4924 and processed for immunofluorescent labeling. Labeled cells were visualized by standard confocal microscopy. Aberrant large COPII-KLHL12 structures were formed upon the MLN4924 treatment. (B) 293 cells stably expressing the indicated construct were processed for immunofluorescent labeling. Labeled cells were visualized by standard confocal microscopy. Large structures that are co-stained with KLHL12 and SEC31A were marked with closed arrowheads. Those that are deficient with SEC31A labeling were marked with open arrowheads.

Figure 3. Regulation of cellular COL1A1 levels by MLN4924. (A) Rapid depletion of intracellular collagen was observed in human skin fibroblasts (HSFs) after cycloheximide

treatment. (B) HSFs were plated and incubated for 24h. Afterwards, the culture medium was replaced with fresh medium with or without MLN4924 (1μM). Conditioned media and cells were collected at indicated times and processed for immunoblotting. The amount of a medium loaded into the gel was normalized to the amount of total proteins in a cell lysate. Riboporin I was probed as a loading control. Medium, unconditioned medium; closed arrowhead, ned-CUL3; open arrowhead, unneddylated-CUL3. (C, D) Quantification of levels of secreted (C) and intracellular (D) collagen. Protein bands were quantified using ImageJ. Student's t-test: P*<0.05, n=3. (E, F) Depletion of KLHL12 (E) or CUL3 (F) by siRNA. Asterisks represent nonspecific proteins. Occasionally, a proteolytic processing of collagen occurs in the secreted collagen, resulting in a fast migrating species (open arrowheads). Note that the reduction in the levels of KLHL12 or CUL3 already reached the maximum at the lowest siRNA concentration used.

Figure 4. Regulation of COL1A1, PERK, and IRE1α levels by CUL3. (A-G) HSFs were transfected with scrambled (Scr) or CUL3 siRNAs. When the cells were incubated with siRNAs and transfection reagents (about 16 h), 10% FBS was absent or present as indicated. The culture medium was then replaced with a fresh complete medium containing 10% FBS. The cells and the conditioned media were collected after additional 48 h of incubation. (A) A representative immunoblot images. (B-D, F-H) Immunoblots images of 4-5 independent experiments were quantified. Statistical analyses were performed with Student's t-test. Error bars represent standard deviations. (B) Comparison of CUL3 levels normalized to α-tubulin. P*<0.0005; P**<0.0001, n=5. (C) Comparison of intracellular COL1A1 levels. P*<0.0001; P**<0.01, n=5. n.s., non-significant. (D) Comparison of secreted COL1A1 levels. P*<0.005, n=5. n.s., non-significant. (E) Levels of *COL1A1* mRNAs were measured with RT-qPCR and normalized to

levels of *GAPDH* mRNAs. P*<0.005, n=7. (F) Comparison of PERK levels. P*<0.0005; P**<0.0001, n=5. (G) Comparison of IRE1α levels. P*<0.0005; P**<0.0001, n=5. (H) Comparison of phosphorylated (p)-eIF2α levels normalized to total levels of eIF2α. P*=0.001, n=4. n.s., non-significant.

Figure 5. Regulation of IRE1α-signaling by CUL3. (A) HSFs were transfected with scrambled (Scr) or CUL3 siRNAs in the presence of the serum. Cells were treated with 2 mM DTT for an indicated duration. (A) A representative immunoblot images. Upon a DTT treatment, bands of PERK and IRE1α migrated slower than those in the untreated condition due to phosphorylation[34]. (B-H) Immunoblots images of 3 independent experiments were quantified. Statistical analyses were performed with Student's t-test. Error bars represent standard deviations. (B) Comparison of CUL3 levels (normalized to α-tubulin) between presence and absence of DTT at each time point. P*<0.0001; P**<0.005, n=3. (C) Comparison of PERK levels between presence and absence of DTT at each time point. P*<0.005; P**<0.01, n=3. Note that band smearing prevented faithful quantification at 3h. (D) Comparison of IRE1α levels. P*<0.0001; P**<0.005; P***<0.0005, n=3. (E) Comparison of ATF6α levels. (F) Comparison of p-eIF2α levels normalized to total levels of eIF2α. P*<0.05, n=3. (G) Comparison of spliced (s) XBP1 levels. P*<0.05; n=3. (H) Comparison of ATF6α NTF levels.

Figure 6. A tissue-specific regulation of the UPR by CUL3. (A, B, and C) Different cell lines were transfected with scrambled (Scr) or CUL3 siRNAs in the absence of the serum.

Immunoblots were quantified for IMR90 cells (B) and for HeLa cells (C). Statistical analyses were performed with Student's t-test. Error bars represent standard deviations. (B) P*<0.05, P**<0.0001, n=4. (C) P*<0.05; P**<0.005, n=4. (D) A model explaining the cell line-specific regulation of the UPR by CUL3 and its adaptors. TC, transcription; TL, translation.

Figure 7. Regulation of COL1A1, PERK, and IRE1α levels by KLHL12. HSFs were transfected with scrambled (Scr) or KLHL12 (K12) siRNAs as described in the legend of Fig. 4. (A) A representative immunoblot images. (B-F) Immunoblots images of 3 independent experiments were quantified. Statistical analyses were performed with Student's t-test. Error bars represent standard deviations. (B) Comparison of KLHL12 levels normalized to α-tubulin. P*<0.0005; n=3. Note that KLHL12 levels were increased in the presence of the serum for unknown reasons. (C) Comparison of intracellular COL1A1 levels. P*<0.005, n=3. (D) Comparison of secreted COL1A1 levels. P*<0.05, n=3. (E) Comparison of PERK levels. P*<0.0001, n=3. n.s., non-significant. (F) Comparison of IRE1α levels. P*<0.0001, n=3.

Figure 8. KLHL41 is responsible for PERK regulation in C2C12 mouse myotubes (CMTs). C2C12 mouse myoblasts were transfected with scrambled (Scr) or indicated siRNAs in a differentiation medium at day 0. The medium was replaced with a fresh differentiation medium at day 1. Cells were harvested at day 3. (A) A representative immunoblot images. For unknown reasons, a depletion of CUL3 led to a reduction of KLHL41 levels, but not vice versa. (B-E) Quantifications of 3 independent experiments were plotted. Statistical analyses were performed with Student's t-test. Error bars represent standard deviations. We were not able to measure

COL1A1 levels because its expression was dramatically reduced in myoblast subcultures. (B) Comparison of CUL3 levels (normalized to α-tubulin). P*<0.005, n=3. (C) Comparison of KLHL41 levels. P*<0.01, P**<0.0001, n=3. (D) Comparison of PERK levels. P*<0.005, P**<0.0001, n=3. (E) Comparison of IRE1α levels.

Figure 1

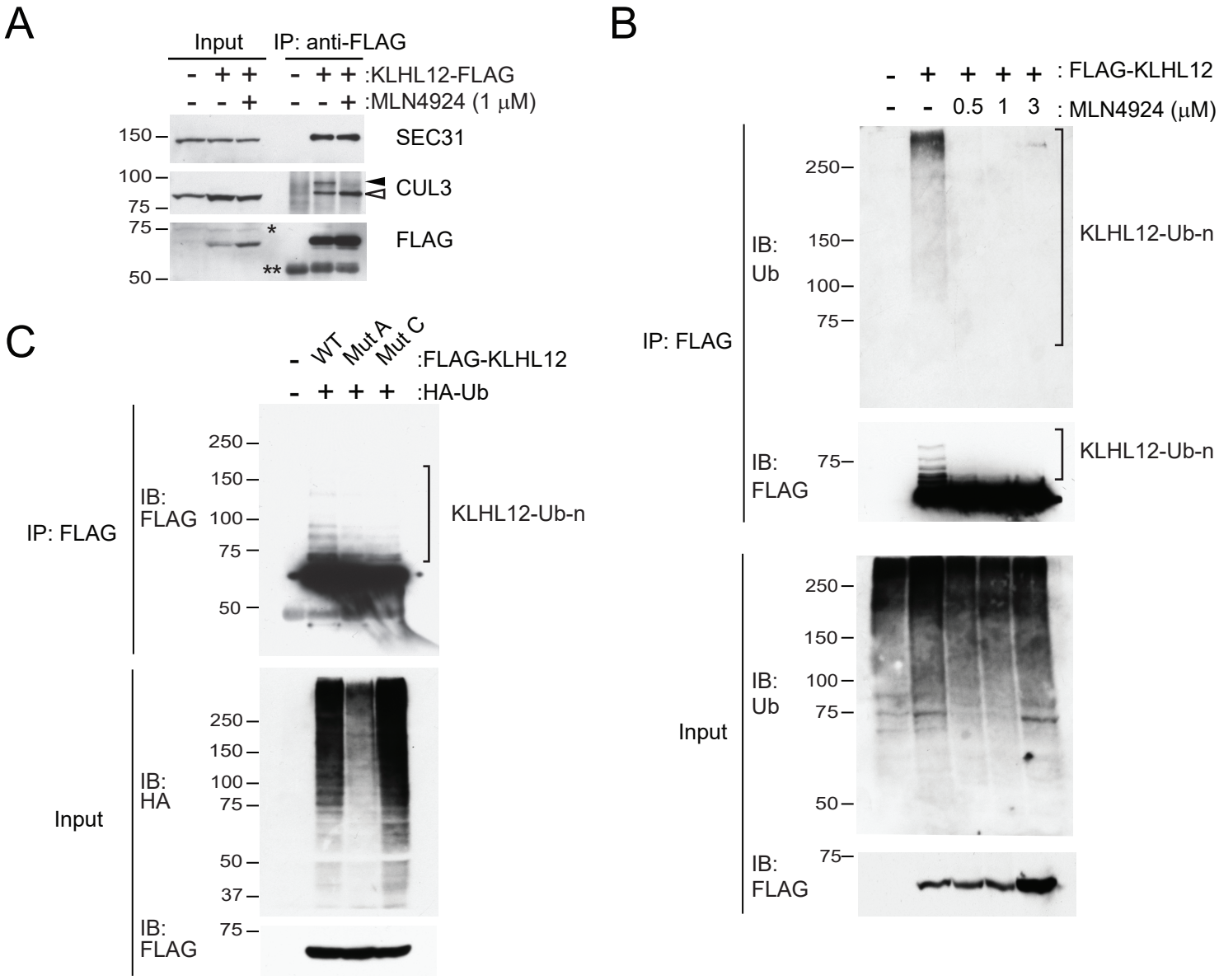

Figure 2

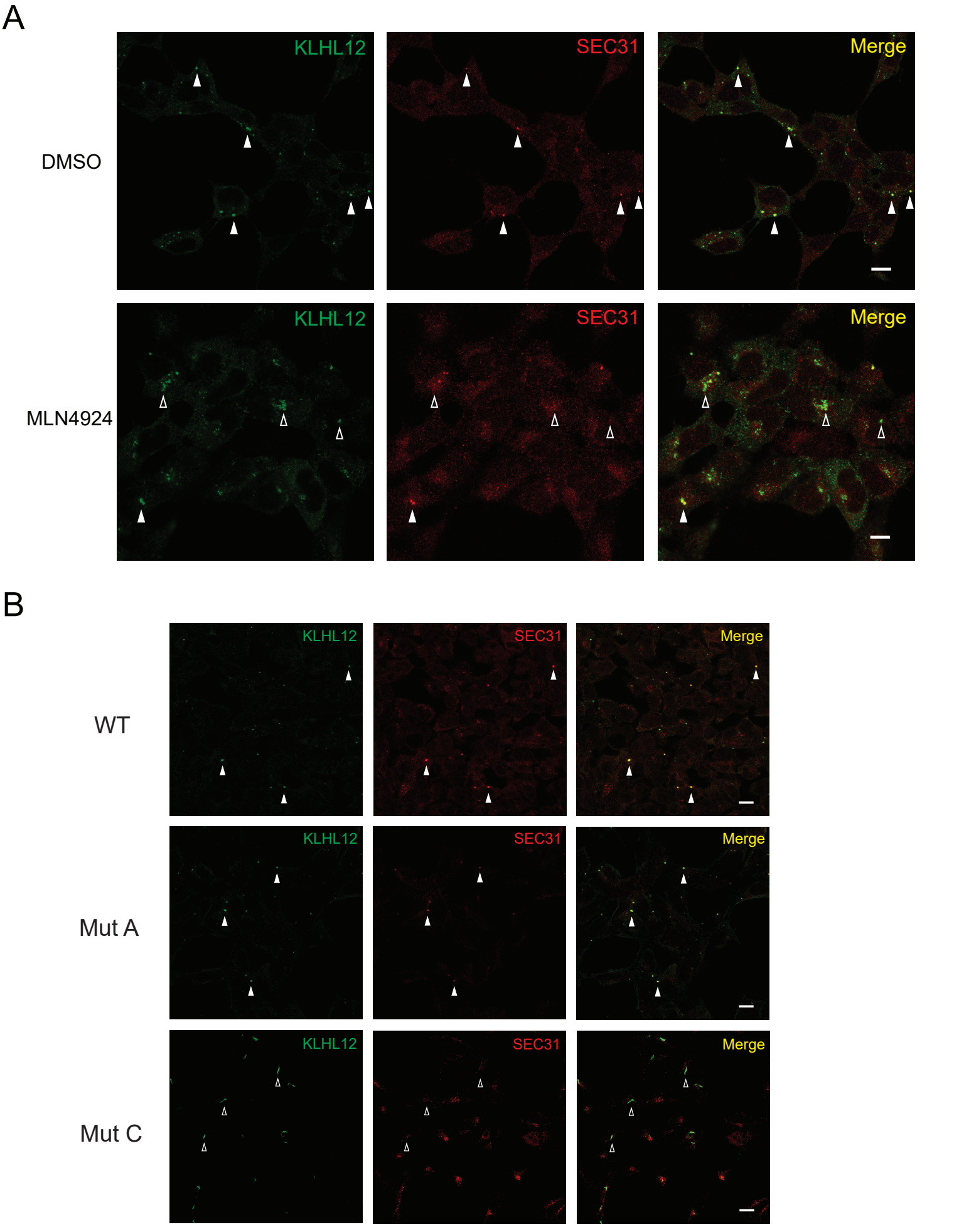

Figure 3

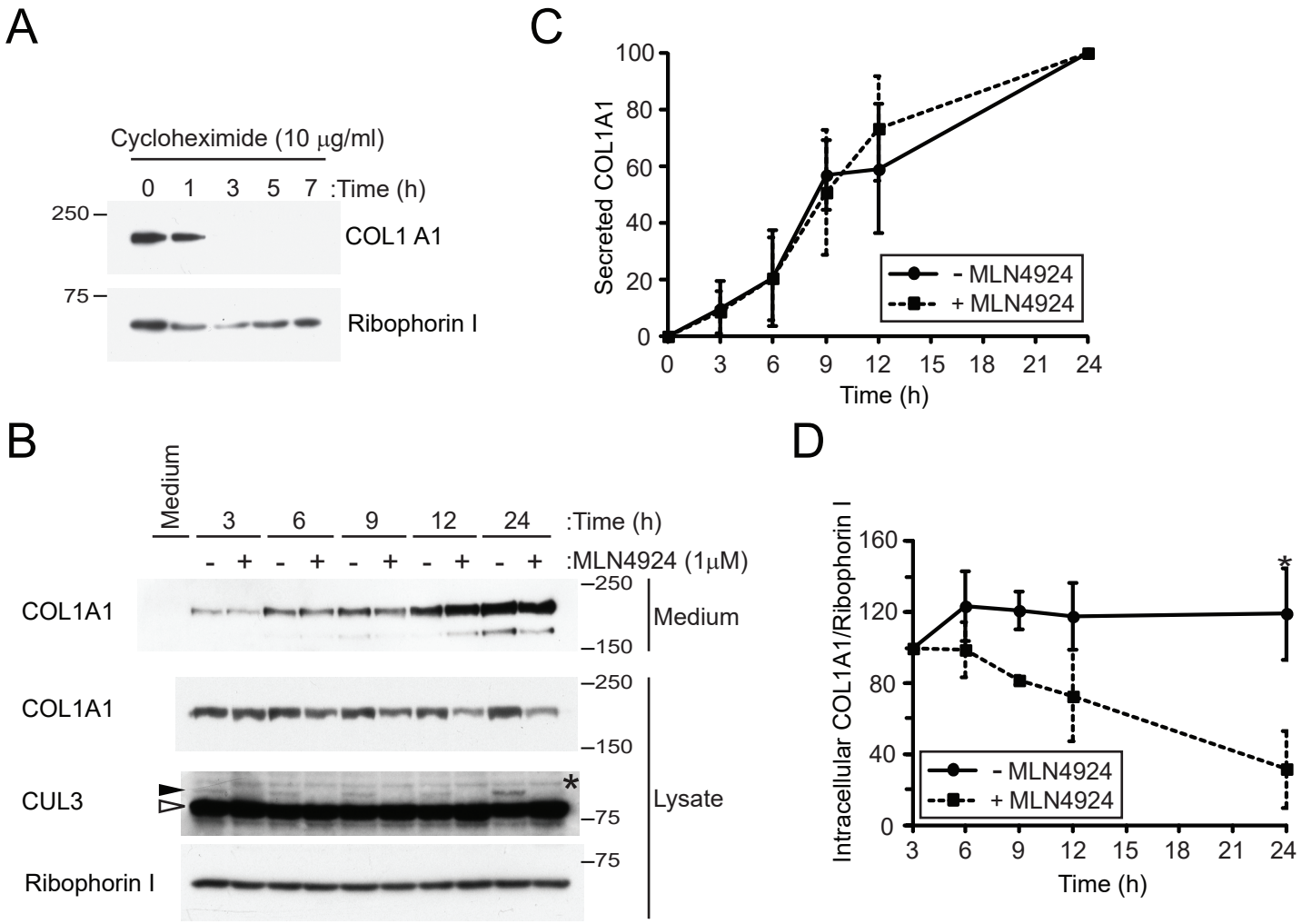

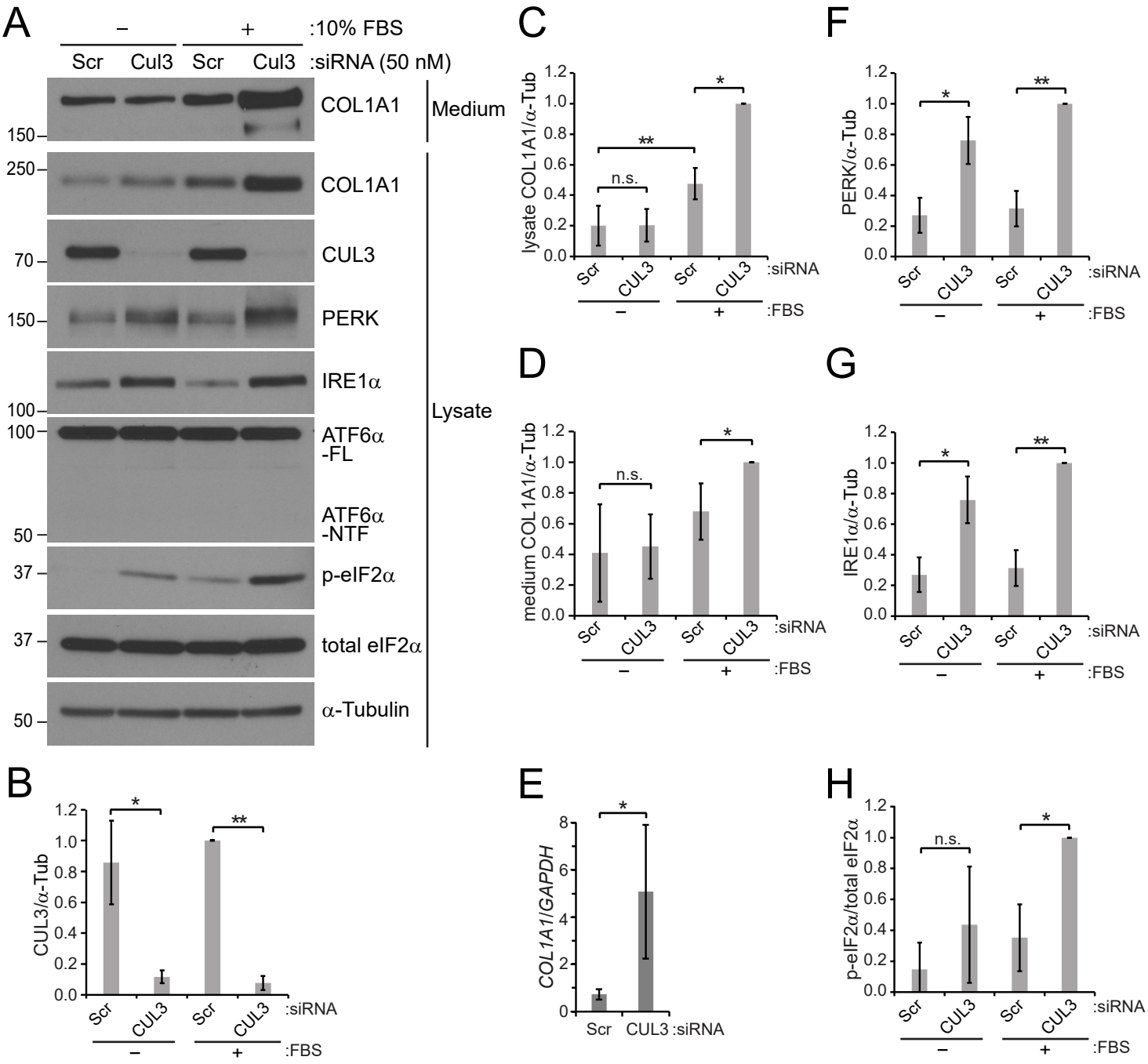

Figure 5

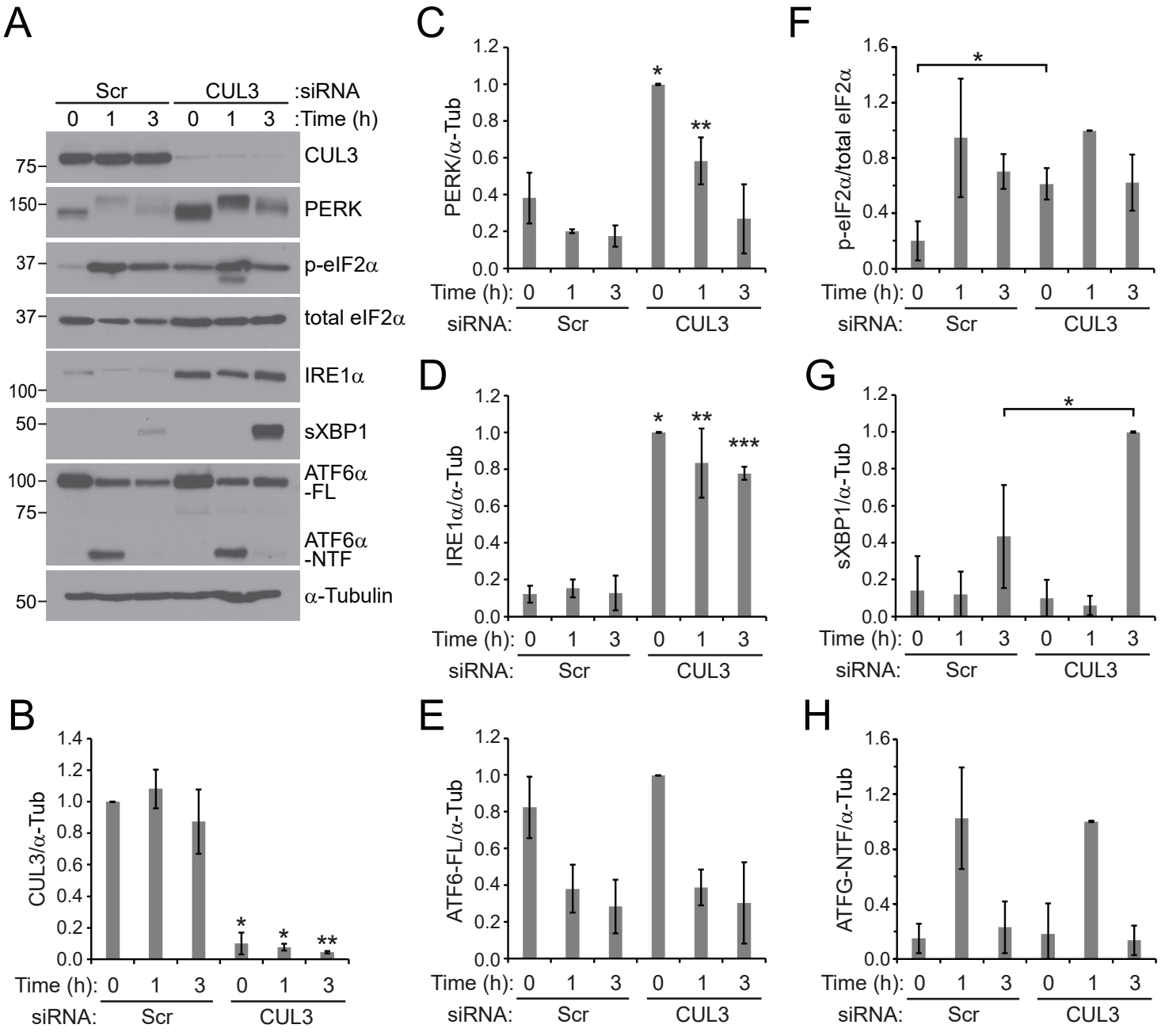

Figure 6

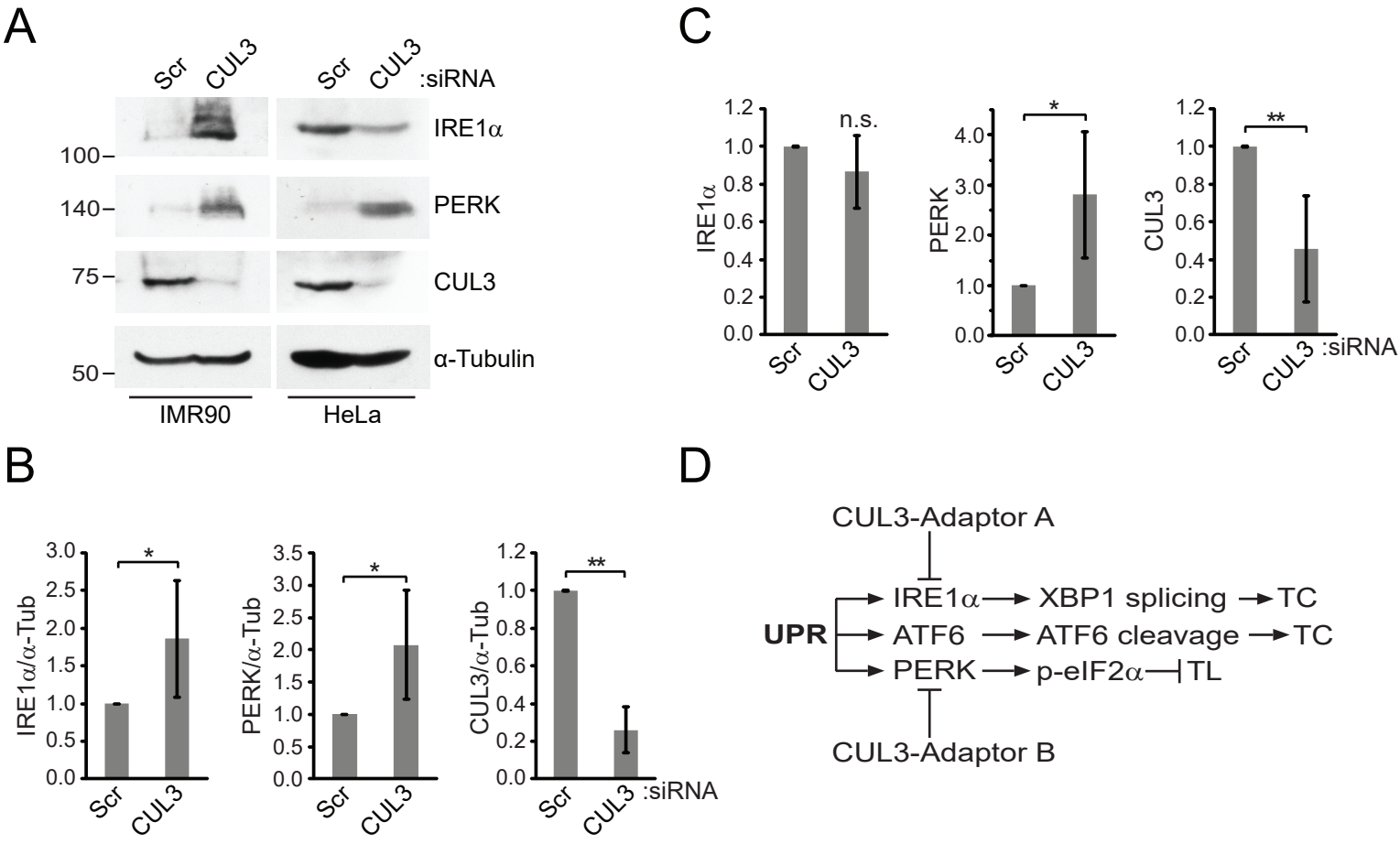

Figure 7

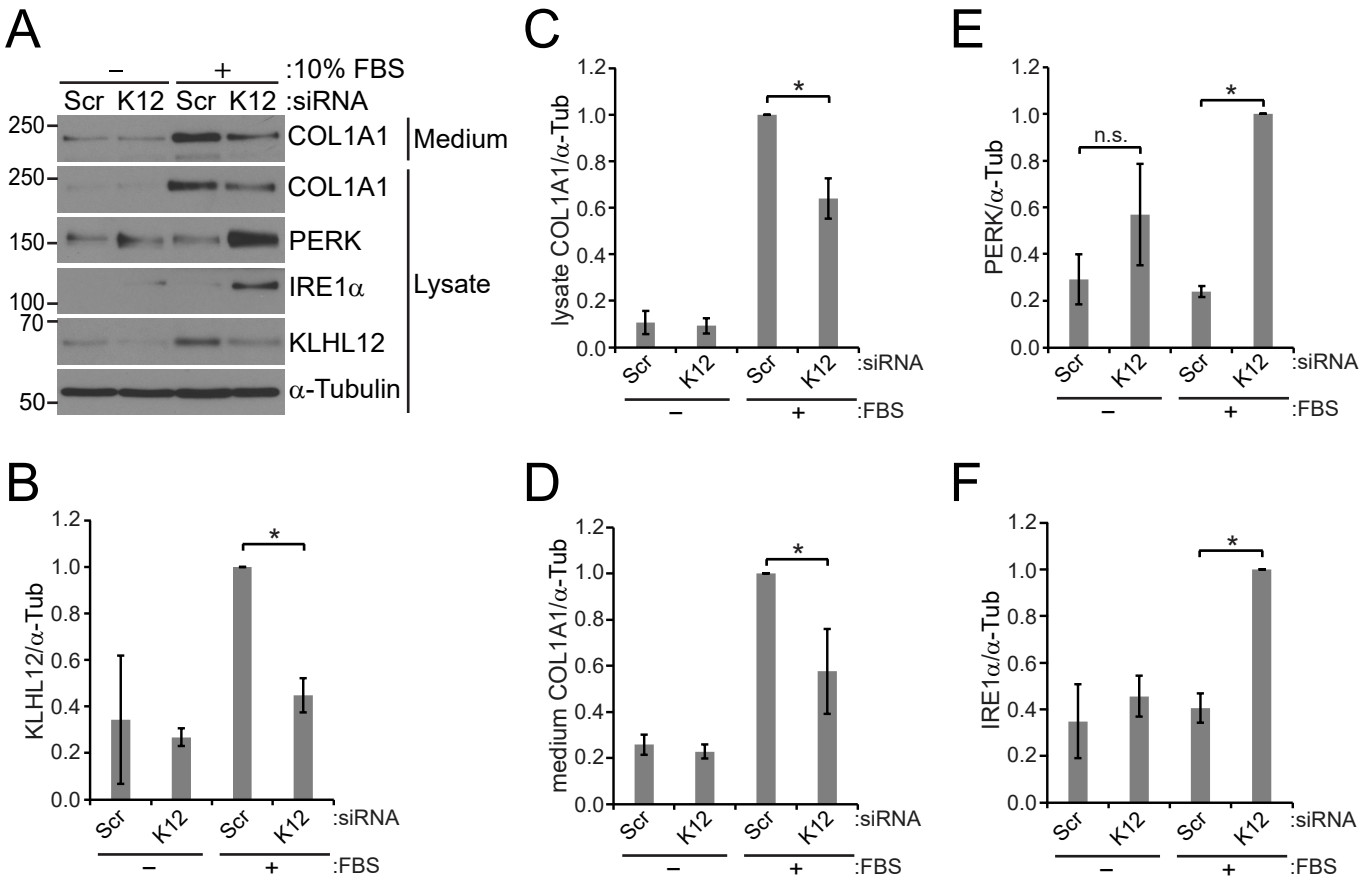

Figure 8